Nuclear Engineering and Technology 51 (2019) 784–791

Contents lists available at ScienceDirect

Nuclear Engineering and Technology

journal homepage: www.elsevier.com/locate/net

Original Article

Distinct properties of tungsten austenitic stainless alloy as a potential nuclear engineering material

E. Salama [a, b, *], M.M. Eissa [c], A.S. Tageldin [b]

[a] Physics Department, Faculty of Science, Ain Shams University, Cairo, Egypt
[b] Basic Sciences Department, Faculty of Engineering, The British University in Egypt (BUE), Egypt
[c] Steel Technology Department, Central Metallurgical Research and Development Institute (CMRDI), Helwan, Egypt

ARTICLE INFO

Article history:
Received 13 July 2018
Received in revised form
12 December 2018
Accepted 24 December 2018
Available online 3 January 2019

Keywords:
Austenitic stainless steel
Tungsten
Microstructure
Mechanical properties
Gamma and neutron shielding

ABSTRACT

In the present study, a series of tungsten austenitic stainless steel alloys have been developed by interchanging the molybdenum in standard SS316 by tungsten. This was done to minimize the long-life residual activation occurred in molybdenum and nickel after decommissioning of the power plant. The microstructure and mechanical properties of the prepared alloys are determined. For the sake of increasing multifunction property of such series of tungsten-based austenitic stainless steel alloys, gamma shielding properties were studied experimentally by means of NaI(Tl) detector and theoretically calculated by using the XCOM program. Moreover, fast neutrons macroscopic removal cross-section been calculated. The obtained combined mechanical, structural and shielding properties indicated that the modified austenitic stainless steel sample containing 1.79% tungsten and 0.64% molybdenum has preferable properties among all other investigated samples in comparison with the standard SS316. These properties nominate this new composition in several nuclear application domains such as, nuclear shielding domain.

© 2018 Korean Nuclear Society, Published by Elsevier Korea LLC. This is an open access article under the CC BY-NC-ND license (http://creativecommons.org/licenses/by-nc-nd/4.0/).

1. Introduction

Stainless steel is an alloy of iron and carbon with at least 10.5% chromium content to have corrosion resistance property. The microstructure of stainless steel alloy depends on its specific amounts of alloying elements. Based on the specific amounts of alloying elements which control their microstructures; five groups stainless steels are commonly obtained. Austenitic stainless steels have face-centred cubic structure while ferritic/martensitic steels have body-centred cubic. Austenitic stainless steels, are one of several structural engineering materials have been recommended as applicant structural materials for nuclear fusion reactors [1,2]. Austenitic stainless steels have been considered as important applicant structural materials for nuclear fusion reactors due to their excellent mechanical properties, excellent manufacturability, welding ability, and corrosion resistance in aqueous solutions and water at high temperatures [3] and extremely shock-resistant. Recently, using both austenitic and ferritic phases as duplex stainless steels have been constructively considered as the structural nuclear material due to their better corrosion resistance and higher mechanical strength than a single phase of austenitic stainless steels [4].

The idea of developing new multifunctional nuclear materials finds increasing interest in recent years [5]. Nuclear materials for advanced nuclear plants must be able to operate under demanding exposure conditions such as temperature, radiation and corrosive media. Stainless steels are robust materials with good corrosion resistance credit to the thin oxide layer formed by chromium [6,7]. Due to its distinct mechanical properties such as, toughness and formability, high strength, large surface area, and excellent physical and thermal properties, stainless steels become suitable as nuclear reactor materials [8,9]. Mn-bearing austenitic stainless steel pipes are used as a part of the conductor jacket of the International Thermonuclear Experimental Reactor (ITER) Central Solenoid (CS) coils due to their lower thermal expansion coefficient [10]. Austenitic stainless steels, such as type 316LN, are used in the high temperature segments such as reactor pressure vessels and primary piping systems [11].

While using austenitic stainless steels type 316 containing Mo and Ni in reactor application some restrictions are combined such

* Corresponding author. Physics Department, Faculty of Science, Ain Shams University, Cairo, Egypt.
E-mail address: e_elsayed@sci.asu.edu.eg (E. Salama).

https://doi.org/10.1016/j.net.2018.12.021
1738-5733/© 2018 Korean Nuclear Society, Published by Elsevier Korea LLC. This is an open access article under the CC BY-NC-ND license (http://creativecommons.org/licenses/by-nc-nd/4.0/).

as activation occurred for Mo and Ni due to neutron exposure. This activation is characterized by the production of long-life residual activation elements after decommissioning of the power plant. Evaluation of irradiation behavior of austenitic stainless steel 316 in Fast Breeder Test Reactor (FBTR) indicated that, beyond 80 dpa; void swelling and associated dimensional changes have occurred as dominant limiting factors [12]. For this reason, Mo and Ni elements must be completely removed and replaced by suitable alloying elements or reduced to the extent that low activation austenitic stainless steel alloy is obtained and the other recommended properties of this alloy are reserved.

Tungsten (W) is usually added to steels as strong ferrite former to improve their mechanical properties. Increasing the steel hardenability and yield strength, which was accompanied by decreasing elongation and Charpy impact energy were observed in some steel alloys as a result of adding W [13–15]. When Tungsten is added to steel alloys, Tungsten carbide is formed. On the other hand, when tungsten is added to steels containing other carbide forming elements such as Mo, Cr and V, it may form complex carbides which increase the amount of undissolved carbides in steel matrix. Tungsten addition was found to produce a larger carbide volume than the other alloying elements at the same C-content [16]. The consequence is the precipitation of fine or very fine carbides distributed in the steel matrix. Complex carbides are capable for retaining a finer grained steel microstructure by retarding the grain growth during heat treatment process. Previous results showed that, in the solution annealed condition, tungsten additions to super duplex stainless steels had a marked positive effect on pitting and crevice corrosion resistance [17]. Tungsten has also been used as a substitution of Mo in duplex stainless steels to improve the corrosion resistance and to prevent sigma phase precipitation during the welding thermal cycle [18].

Nuclear materials used for gamma radiation shielding should have high gamma attenuation coefficient, possess good mechanical properties, long-term reliability, good fabrication, a small radiation defects, and joining properties with suitable thermo-physical characteristics [19,20]. Increasing the gamma attenuation property of austenitic stainless steel alloys will increase its multifunctional use in several nuclear reactor applications. In the radiation shielding domain, containers made of AISI 304L stainless steel can be used for the temporary storage of low and medium level radioactive waste for a period of 30 years [21].

The main objective of the present work is to develop low activation austenitic steel alloy with comparable high gamma attenuation coefficient. The developed alloy is based on substituting tungsten (W) on the expense of molybdenum (Mo) in the conventional higher activation SS316 austenitic stainless steel to minimize the long-life residual activation occurred after decommissioning of the power plant. The obtained results may also nominate the prepared alloy to be used in nuclear material applications such as, radiation shielding domain and high-temperature segments in reactor pressure vessels and primary piping systems.

2. Material and methods

2.1. Samples preparation

A series of tungsten austenitic stainless steel alloys have been prepared by replacing the molybdenum by tungsten in standard stainless steel SS316. Sample preparations were carried out using a medium frequency induction furnace including 30 kg pilot-plant furnace at CMRDI. Six melts were carried out. In the first melt, a standard sample (AISI 316) was designed to be produced. In other four melts, molybdenum was partially replaced by tungsten, while in the last melt, molybdenum was mostly eliminated and replaced by tungsten. The tungsten content has been adjusted by adding ferrotungsten. For the sake of increasing the hardness, the hot forged steels samples in the shape of solution were firstly annealed at 1050 °C for about 30 min, followed by water quenching [22]. Iron molds of inner diameter 70 mm have been used to shape the melts. The prepared samples are finally formed to be 30×30 mm^2 cross-sectional bars. Table 1 contains the chemical compositions of the prepared samples.

The metallographic examinations were carried out using cylindrical specimens cut out from the produced solution treated steels. The specimen's surface is ground on 100, 240, 400, 800, 1200 and 2000 grade emery papers and polished on alumina paste. The microstructure is observed using an Olympus light microscope after electrochemically etching in an oxalic acid solution (5wt %) in alcohol. Vickers hardness was measured on polished specimens at room temperature with a 5 g load. The average values of Vickers hardness were recorded for every five readings.

The tensile test is carried out using a 10 kN Shimadzu screw -driven universal testing machine at room temperature with constant cross-head velocity of 1 mm/min. Round tensile specimens are machined according to the specification of the ASTM E23 - 16b of 6 mm diameter and 30 mm gauge length.

Ultimate tensile strength, 0.5% proof stress, and elongation to fracture were estimated throughout the tensile test. Three specimens were used for each steel and the average of them was estimated. Standard Charpy V-notch specimens (10 mm $\times$ 10 mm x 55 mm) were prepared according to the specification of the ASTM E 23-16b. Three specimens for each steel were tested at room temperature on AVERY impact-testing machine to measure the energy transferred to the stainless steel samples and the average of them was adopted.

Stability condition and phase identification of the prepared stainless steels samples can be determined by using the Schaeffler diagram based on what is called nickel and chromium equivalents. Nickel and chromium equivalents for stainless steels alloys can be calculated by using the following formulas [23].

$$Ni_{Equi} = Ni + 0.5Mn + 30C + 0.3Cu + Co \quad (1)$$

$$Cr_{Equi} = Cr + 1.5Si + 1.5Mo + 5V + 1.5Ti + 1.75Nb + 5.5Al + 0.75W \quad (2)$$

The indicated elements in these expressions are referred to their concentrations weight percentages.

Gamma-ray attenuation coefficients of the prepared samples are measured at five gamma energy lines (238.63, 338.28, 583.19, 911.2 and 2614 keV) emitted from ^{232}Th radioactive source. The attenuation coefficient at 2614 keV gamma energy line has special importance in the reactor design circumstances, because of the fact that the reactor total gamma rays yield lies in the range of 2–8 MeV with an average value of 4 MeV [24]. "2x2" NaI (Tl) scintillation of good geometry was used to measure γ-ray attenuation coefficients. To compare the obtained experimental results with those theoretical calculated, XCOM online program (https://physics.nist.gov/cgi-bin/Xcom/xcom2) can be used to calculate the mass attenuation coefficient of the prepared stainless steel samples at different energies [25].

2.2. Theoretical calculations

The mass attenuation coefficient (μ_m) at any photon energy of compound or mixture can be determined by using the Beere Lambert law as:

Table 1
Prepared alloys elemental composition (wt %) and relative densities.

Elements	Steel Code					
	SS316	SSW1	SSW2	SSW3	SSW4	SSW5
C	0.05	0.08	0.08	0.08	0.08	0.08
Si	0.63	0.37	0.61	0.31	0.33	0.33
Mn	0.99	0.64	0.71	0.48	0.71	0.71
P	0.025	0.01	0.025	0.02	0.034	0.014
S	0.005	0.018	0.031	0.029	0.03	0.034
Cr	17.5	16.39	16.78	16.3	16.5	16.06
Ni	11.77	11.43	10.86	11.3	11.6	11.82
Al	0.015	0.013	0.013	0.011	0.009	0.004
Co	0.22	0.15	0.15	0.19	0.15	0.18
Cu	0.14	0.07	0.06	0.07	0.06	0.07
Nb	0.003	0.002	0.011	0.011	0.008	0.008
Ti	0.003	0.003	0.004	0.004	0.003	0.004
V	0.06	0.1	0.11	0.1	0.13	0.1
Fe	66.379	68.484	68.206	68.815	67.926	68.206
Mo	2.2	1.67	1.18	0.75	0.64	0.14
W	0.01	0.57	1.17	1.53	1.79	2.24
Relative Density	7.88	7.947	7.98	8.037	8.062	8.109

$$I = I_0 e^{-\mu_m \rho x} \quad (3)$$

where, I_0 and I are unattenuated and attenuated photon intensities, μ_m ($cm^2 g^{-1}$) is the mass attenuation coefficients, x (cm) is the sample thickness, and ρ (g cm^{-3}) is the density of the material.

The attenuation of neutrons in a material of thickness x (cm) and total macroscopic cross -section Σ_t can be calculated by the following law [26].

$$I = I_o e^{-\Sigma_t x} \quad (4)$$

Where I_o and I are the intensities of ingoing and outgoing neutrons respectively.

Attenuation of fast neutron through materials means removal from the fast group and in this case, the elastic scattering is the most probable interaction of a fast neutron and other interactions are negligible. Therefore, removal cross-section parameter denoted by $\sum_R$ (cm^{-1}) could be used in case of fast neutron attenuation. Removal cross section is a fraction from the total macroscopic cross-section [27]. The removal cross section of neutrons is one of the most important parameters to choose the reactor core materials.

3. Results and discussions

The calculated Nickel and chromium equivalents for the prepared stainless steel alloys are listed in Table 2. Schaeffler diagram including the prepared samples and the standard SS316 is shown in Fig. 1. This diagram predicts that the developed tungsten stainless steels SSW1, SSW3, SSW4 and SSW5 have a single austenite phase while SSW2 and the standard stainless steel SS316 reveal mainly austenite phase with low contribution of ferrite (5–7%).

The X-ray powder diffraction (XRD) was recorded for the prepared alloys SSW2, SSW4, SSW5 and the standard SS316 to investigate the produced phases. The XRD analysis was performed with

Table 2
Cr and Ni equivalents for the studied stainless steel alloys.

	SS316	SSW1	SSW2	SSW3	SSW4	SSW5
Cr equivalent (wt. %)	22.14	20.455	20.976	19.610	20.006	18.977
Ni equivalent (wt. %)	14.02	14.321	13.783	14.151	14.523	14.776

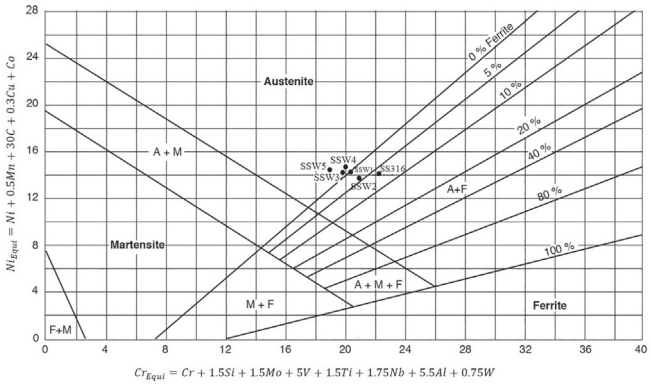

Fig. 1. Schaeffler diagram of the investigated stainless steel alloys.

Philips X'pert Pro X-ray powder diffractometer using Cu Kα radiation (1.5418 A) at a scanning speed of 0.3 s. According to PDF2: 00-023-0298 reference code, the austenitic stainless steel peaks are obtained in all the investigated alloys at (111), (200), (220), (311) and (222) with cubic structure as shown in Fig. 2. No other phases can be observed such as MO-carbide and W-carbide due to their low weight percent.

The optical micrographs of the studied samples are given in Fig. 3. The investigation of these photos indicated that, all samples have mainly austenite stainless steel structure and contain a large

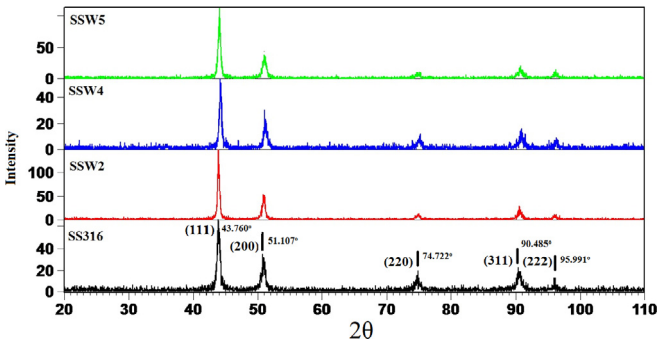

Fig. 2. X-ray diffraction (XRD) results for the prepared alloys.

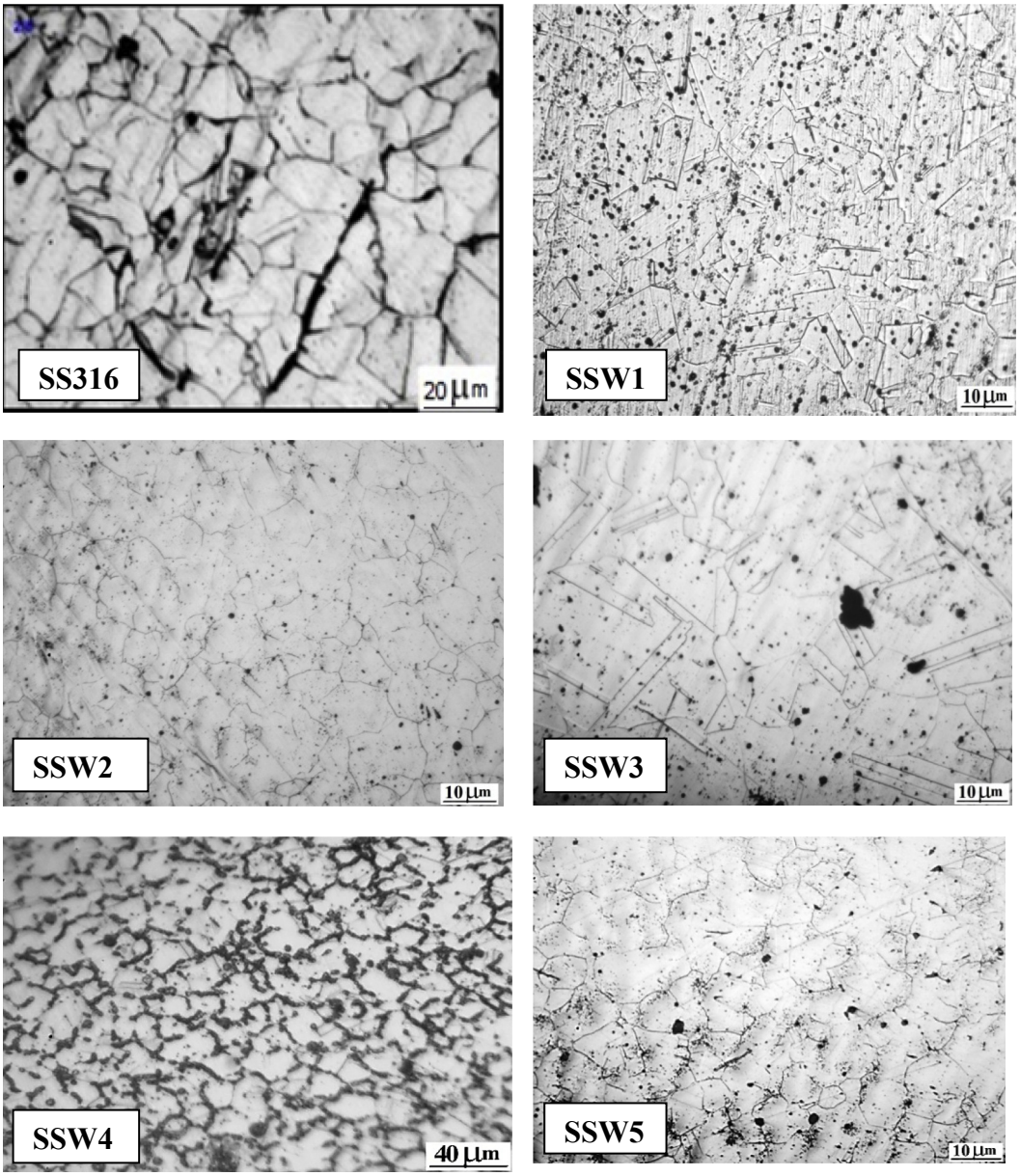

Fig. 3. Microstructure of investigated stainless steels.

number of twins which characterize the appearance of the austenitic stainless steel. The addition of W has significantly changed the austenite grain size and retarding the growth of austenite grains [14]. As shown in Fig. 3 from SSW1 to SSW5, increasing the W content leads to finer austenite grain size shown in SSW4 sample compared with the other samples of lower W contents.

Solution annealing at 1050 °C is usually applied to austenite stainless steels. In the present study, this temperature seems to be enough to take all Mo into solution. However, for W-bearing stainless steels in which W is a strong carbide former with lower solubility, it is concluded that the final annealing temperature is not high enough for a fully solid solution, and a portion of W-carbide still exist which hasn't taken into solution. Solution annealing at 1050 °C used in the present study, seems to be not high enough for all Mo and W complex carbides to pass into the solid solution.

Fig. 4 shows the influence of tungsten content on the hardness of the investigated stainless steels. Increasing the W/(W+Mo)

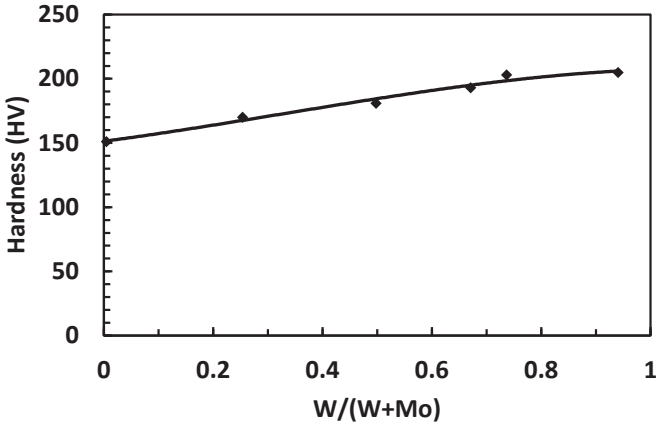

Fig. 4. Hardness variation of the investigated tungsten stainless steel versus tungsten ratio to tungsten and molybdenum.

Table 3
Mechanical parameters of the prepared samples.

Steel Code	W/(Mo+W)	Vickers Hardness (HV)	Yield Strength (MPa)	Ultimate Strength (MPa)	Elongation (%)	Impact Energy (J)
SS316	0.005	151	639.8	737.4	30.2	272
SSW1	0.254	170	642.4	733.1	28.7	153
SSW2	0.498	181	807.9	844.8	20.2	138
SSW3	0.671	193	799.7	861.2	23.5	149
SSW4	0.737	203	911.5	973.2	23.9	181
SSW5	0.941	185	635.4	745.7	25.0	142

content generally increases the hardness values of the specimens. This hardness increment could be attributed to the solid solution hardening of tungsten and the higher strengthening effect of complex tungsten-molybdenum carbides as compared with molybdenum carbide. However, high reduction of Mo content, in which W substitutes that reduction results in decreasing the hardness. This behavior may be attributed to higher hardening effect of complex W-Mo-carbides compared with either single Mo- or W- carbides.

Table 3 contains the obtained results concerning the Ultimate Tensile Strength (MPa), Elongation (%), Vickers Hardness (HV), Yield Strength (MPa), and impact energy (J). Yield stress and ultimate tensile show an inverse behavior compared to elongation in which the yield stress and ultimate tensile increase and elongation decreases with a mirror-like pattern as a function of W/(W+Mo) content as shown in Fig. 5, Fig. 6 and Table 3. T.

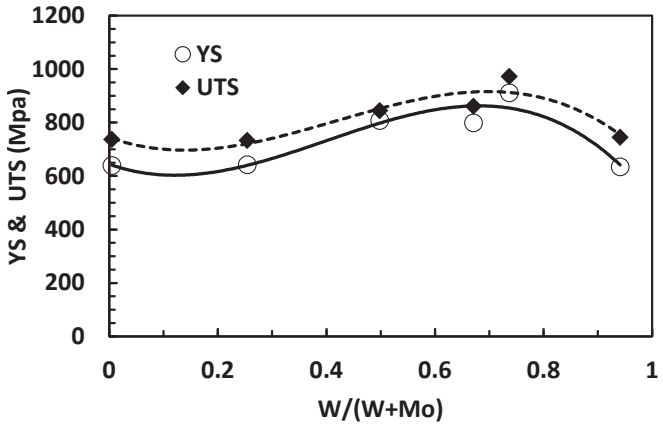

Fig. 5. Yield Stress and ultimate tensile stress versus tungsten ratio to tungsten and molybdenum.

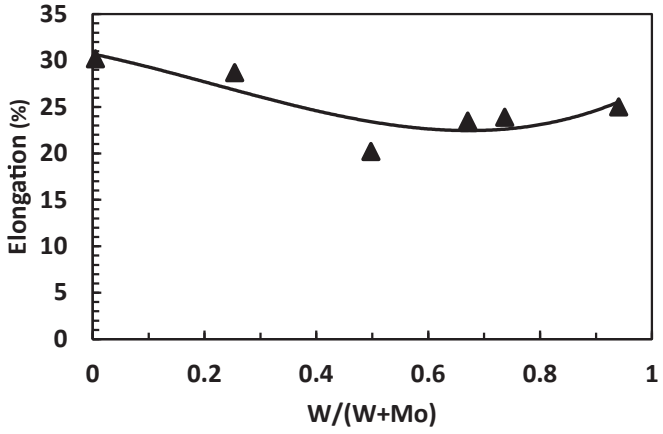

Fig. 6. Elongation test results versus tungsten ratio to tungsten and molybdenum.

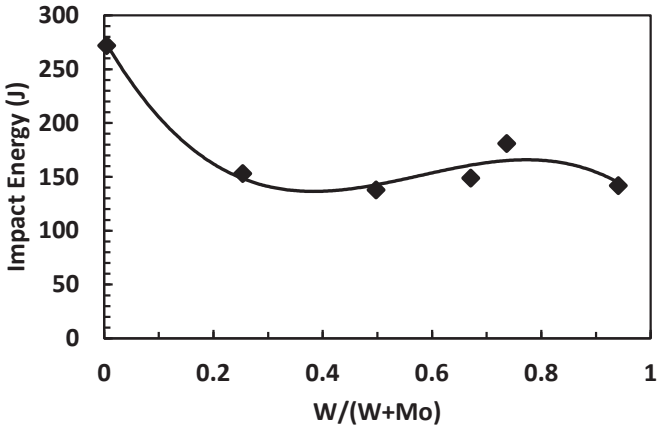

Fig. 7. Impact Energy test versus tungsten ratio to tungsten and molybdenum.

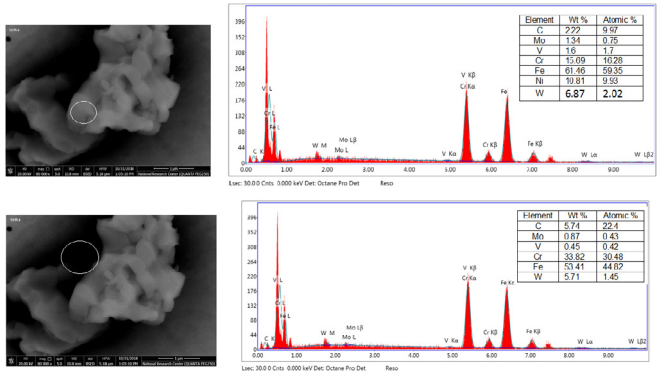

Fig. 8. SEM-EDX scan for SSW4-prepared alloy.

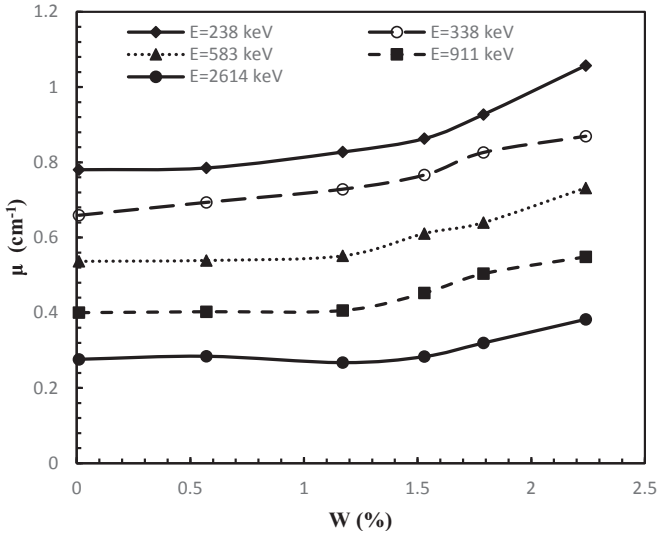

Fig. 9. Linear attenuation coefficients versus tungsten concentration at different energies (E).

The higher strengthening of modified Mo-W-austenitic stainless steels could be attributed to the finer microstructure, solid solution hardening of Tungsten and the higher strengthening effect of W-Mo-complex carbides. The highest strength is obtained at W/(W+Mo) equals 0.74. However, total replacement of molybdenum by tungsten leads to decrease the strength to the level of single Molybdenum additive steel. This trend confirms the higher strengthening effect of complex tungsten-molybdenum carbides compared with either molybdenum or tungsten carbide.

Fig. 7 shows the relation between the ability to stand for impacts as a function of the tungsten to tungsten and molybdenum ratio. As it is clear from this figure, replacement of molybdenum by tungsten decreases the impact energy, which could be attributed to the brittle effect of W- and W-Mo- carbides. However, the modified tungsten-stainless steels still exhibit high impact energy. These findings are confirmed by some previous studies regarding the effect of adding tungsten on the mechanical properties of stainless steel alloys. It was found that, addition of W increases both the hardness and the tensile strength at the expense of elongation and Charpy impact energy [14,28]. For the Fe-8Mn-7Ni-W alloys, the

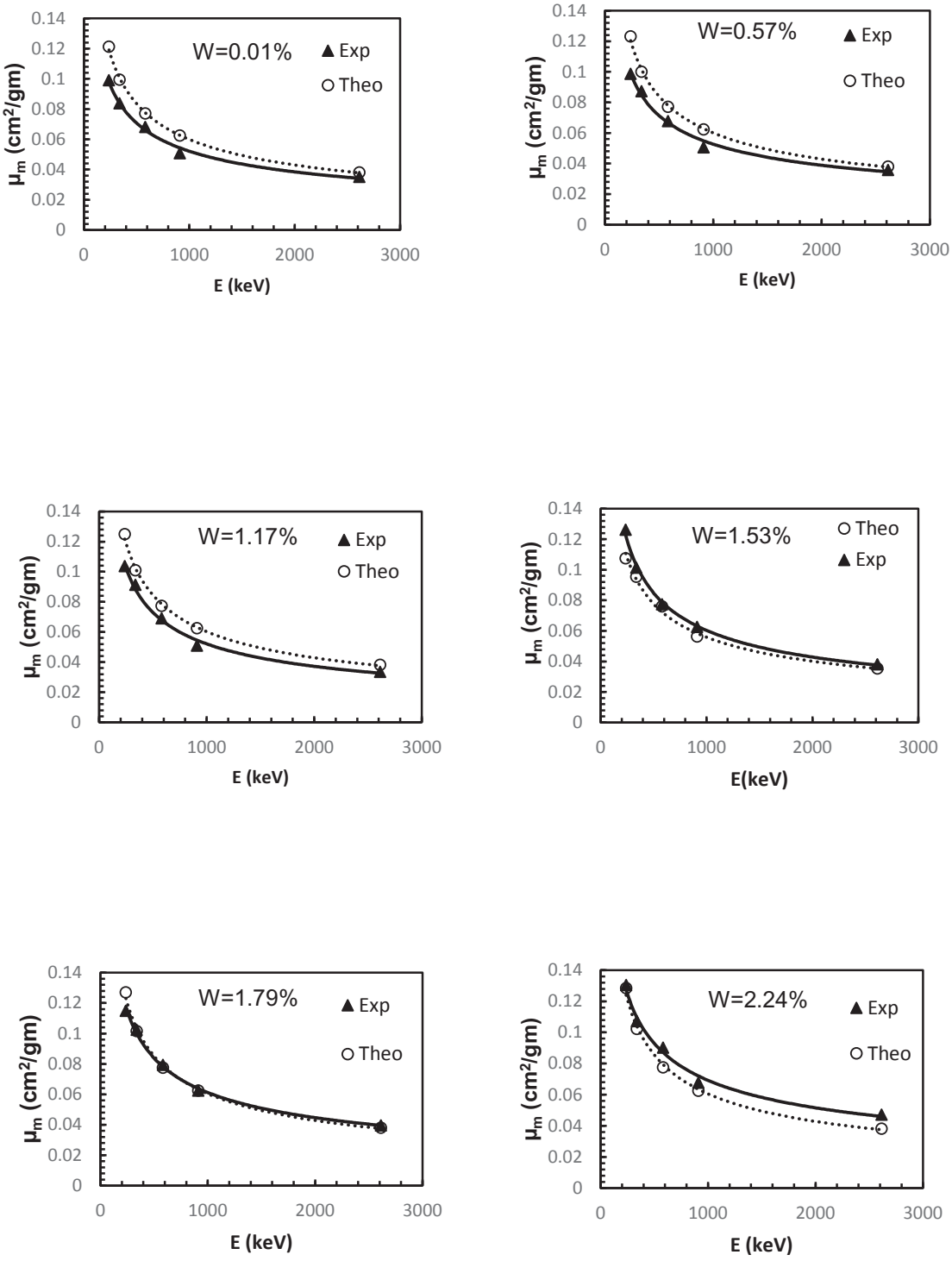

Fig. 10. Mass Attenuation coefficients (μ_m) as a function of gamma ray energy (E) for different tungsten concentrations (W%).

Table 4
The calculated effective mass removal cross-section of the prepared stainless steel alloys.

Sample code	Mass removal cross section ($cm^2\ g^{-1}$)
SS316	0.015127
SSW1	0.015090
SSW2	0.015086
SSW3	0.015054
SSW4	0.015047
SSW5	0.015032

tensile strength significantly increased with increasing W content at the expense of tensile elongation [29].

The existence of carbide phases cannot be proofed by XRD due to the low concentrations of Mo and W. The SEM-EDX scan for SSW4 is performed as shown in Fig. 8. Because of carbon concentrations are very low in all the prepared samples, the indicated high concentration of carbon at the selected scanned regions implies the existence of carbide phases.

The measured attenuation coefficients (μ) of the investigated samples at different γ-rays and for versus tungsten concentration (W %) in the stainless steel system are shown in Fig. 9. The linear attenuation coefficients of all stainless steel samples increase with increasing W- content, and inversely proportional to energy. These behaviors can be attributed to the higher molecular weight of tungsten as well as, the mechanism of gamma ray interaction with the materials.

The measured and calculated values of the mass attenuation coefficients (μ_m) as functions of the gamma-ray energies for five samples containing different tungsten concentrations are shown in Fig. 10. Matching between both results with reasonable small variation can be attributed to the existence of systematic errors; which may be due to non-stoichiometry ratio of the sample formula after melting at high temperature.

The calculated neutron removal cross-section of the prepared steel alloys is listed in Table 4. It was observed that, the calculated mass removal cross section has a slight change which could be endorsed to the variation of cross sections of elements' nuclei and their weight fraction inside each alloy. Additionally, no significant change in the removal cross sections compared with the standard sample (SS316). This can be clarified based on the fact that, all the prepared alloys have a similar chemical composition, nearly the same mass density, and the exchanged elements have nearly the same removal cross section.

The elastic, inelastic, and capture reactions in the studied alloys represent the reduction of fast neutrons removal cross section. The minor change in the removal cross-section may considered due to the gradual increase of the tungsten content in the stainless steel alloys.

4. Conclusions

In the present study, the mechanical, structural and gamma-ray shielding properties of developed tungsten stainless steel alloys are investigated in order to be used in different nuclear applications. The measured mechanical properties such as hardness, yield stress and ultimate tensile strength were increased, while elongation and impact energy was decreased with increasing tungsten ratio at the expense of molybdenum content in standard SS316. The measured mass attenuation coefficients are increased with the increase of W content in the investigated tungsten based stainless steels. The calculated macroscopic neutron removal cross-section of the prepared alloys has a slight change compared with the standard sample. This slight change could be attributed to the gradual increase of the tungsten content in the prepared alloys. The obtained combined mechanical, structural and shielding properties indicate that the austenitic stainless steel SSW4 sample has preferable properties among all other investigated samples where, higher values of hardness, tensile strength and ultimate strength compared with all the prepared alloys and the standard SS316 are observed. In addition, the higher gamma attenuation and comparable neutron removal cross section with lower gamma activation with respect to the standard SS316 are highly recommended. From the obtained results, it can be concluded that the developed alloy SSW4 can be used instead of the standard SS316 in several nuclear applications such as nuclear shielding domain and high-temperature segments in reactor pressure vessels and primary piping systems. However, comprehensive performance can be realized after finalizing the long-term performance test such as corrosion, creep and welding behavior.

References

[1] S. Şahin, M. Übeyli, A review on the potential use of austenitic stainless steels in nuclear fusion reactors, J. Fusion Energy 27 (2008) 271–277, https://doi.org/10.1007/s10894-008-9136-3.
[2] B. Van Der Schaaf, Structural materials requirements for in-vessel components of fusion power plants, Fusion Eng. Des. 51–52 (2000) 43–54, https://doi.org/10.1016/S0920-3796(00)00318-5.
[3] B. Stellwag, The mechanism of oxide film formation on austenitic stainless steels in high temperature water, Corros. Sci. 40 (1998) 337–370, https://doi.org/10.1016/S0010-938X(97)00140-6.
[4] Y. Choi, Y. Baik, B.M. Moon, D.S. Sohn, Corrosion and wear properties of cold rolled 0.087% Gd lean duplex stainless steels for neutron absorbing material, Nucl. Eng. Technol. 48 (2016) 164–168, https://doi.org/10.1016/j.net.2015.10.002.
[5] P. Yvon, F. Carré, Structural materials challenges for advanced reactor systems, J. Nucl. Mater. 385 (2009) 217–222, https://doi.org/10.1016/j.jnucmat.2008.11.026.
[6] V.P. Singh, N.M. Badiger, Gamma ray and neutron shielding properties of some alloy materials, Ann. Nucl. Energy 64 (2014) 301–310, https://doi.org/10.1016/j.anucene.2013.10.003.
[7] M.M. Eissa, S.U. El-kameesy, S.A. El-Fiki, S.N. Ghali, R.M. El Shazly, A. Saeed, Attenuation capability of low activation-modified high manganese austenitic stainless steel for fusion reactor system, Fusion Eng. Des. 112 (2016) 130–135, https://doi.org/10.1016/j.fusengdes.2016.08.002.
[8] T.S. Byun, N. Hashimoto, K. Farrell, Temperature dependence of strain hardening and plastic instability behaviors in austenitic stainless steels, Acta Mater. 52 (2004) 3889–3899, https://doi.org/10.1016/j.actamat.2004.05.003.
[9] K.D. Min, S. Hong, D.W. Kim, B.S. Lee, S.J. Kim, Fatigue crack growth characteristics of nitrogen-alloyed type 347 stainless steel under operating conditions of a pressurized water reactor, Nucl. Eng. Technol. 49 (2017) 752–759, https://doi.org/10.1016/j.net.2017.01.019.
[10] S. Sgobba, P. Libeyre, D.J. Marcinek, A. Nyilas, A comparative assessment of metallurgical and mechanical properties of two austenitic stainless steels for the conductor jacket of the ITER Central Solenoid, Fusion Eng. Des. (2013) 2484–2487, https://doi.org/10.1016/j.fusengdes.2013.05.002.
[11] K. Karthick, S. Malarvizhi, V. Balasubramanian, S.A. Krishnan, G. Sasikala, S.K. Albert, Tensile and impact toughness properties of various regions of dissimilar joints of nuclear grade steels, Nucl. Eng. Technol. (2017), https://doi.org/10.1016/j.net.2017.10.003.
[12] V. Karthik, S. Murugan, P. Parameswaran, C.N. Venkiteswaran, K.A. Gopal, N.G. Muralidharan, S. Saroja, K.V. Kasiviswanathan, Austenitic stainless steels for fast reactors - irradiation experiments, property evaluation and microstructural studies, Energy Procedia (2011) 257–263, https://doi.org/10.1016/j.egypro.2011.06.033.
[13] R.L. Klueh, P.J. Maziasz, The microstructure of chromium-tungsten steels, Metall. Trans. A (1989), https://doi.org/10.1007/BF02653916.
[14] J. Zhao, T. Lee, J.H. Lee, Z. Jiang, C.S. Lee, Effects of tungsten addition on the microstructure and mechanical properties of microalloyed forging steels, Metall. Mater. Trans. A Phys. Metall. Mater. Sci. (2013), https://doi.org/10.1007/s11661-013-1695-x.
[15] S. Prifiharni, M.S. Anwar, A. Nikitasari, E. Mabruri, The hardness, microstructure, and pitting resistance of austenitic stainless steel Fe25Ni15Cr with the addition of tungsten, niobium, and vanadium, AIP Conf. Proc. (2018), https://doi.org/10.1063/1.5038323.
[16] W.C. Leslie, The Physical Metallurgy of Steels, first ed., Hempisphere Pub. Corp, Washington, 1981. New York : McGraw-Hill.
[17] E.B. Haugan, M. Næss, C.T. Rodriguez, R. Johnsen, M. Iannuzzi, Effect of Tungsten on the Pitting and Crevice Corrosion Resistance of Type 25Cr Super Duplex Stainless Steels, Corrosion, 2017, https://doi.org/10.5006/2185.
[18] Jun-ichi Higuchi and Eiki Nagashima, Development of DP28W™ duplex stainless, Stainl. Steel World. (n.d.) 29–32. http://www.stainless-steel-world.

net/pdf/DP28W_duplex.pdf.
[19] M. Bastürk, J. Arztmann, W. Jerlich, N. Kardjilov, E. Lehmann, M. Zawisky, Analysis of neutron attenuation in boron-alloyed stainless steel with neutron radiography and JEN-3 gauge, J. Nucl. Mater. 341 (2005) 189–200, https://doi.org/10.1016/j.jnucmat.2005.02.003.
[20] M. Büyükyıldız, M. Kurudirek, M. Ekici, O. İçelli, Y. Karabul, Determination of radiation shielding parameters of 304L stainless steel specimens from welding area for photons of various gamma ray sources, Prog. Nucl. Energy 100 (2017) 245–254, https://doi.org/10.1016/j.pnucene.2017.06.014.
[21] L. Vehovar, M. Tandler, Stainless steel containers for the storage of low and medium level radioactive waste, Nucl. Eng. Des. (2001), https://doi.org/10.1016/S0029-5493(00)00443-X.
[22] N.M. Ismail, N.A.A. Khatif, M.A.K.A. Kecik, M.A.H. Shaharudin, The effect of heat treatment on the hardness and impact properties of medium carbon steel, IOP Conf. Ser. Mater. Sci. Eng. (2016), https://doi.org/10.1088/1757-899X/114/1/012108.
[23] J. Feldstein, F. Lake, A new constitution diagram for predicting ferrite content of stainless steel weld metals, Mater. Des. 14 (1993) 345–348, https://doi.org/10.1016/0261-3069(93)90110-H.
[24] S.U. El-Kameesy, E. Salama, Radioactive contamination of the atmosphere of Cairo, Egypt, from the Fukushima Dai-ichi nuclear plant accident, Isot. Environ. Health Stud. 49 (2013), https://doi.org/10.1080/10256016.2013.771636.
[25] L. Gerward, N. Guilbert, K.B. Jensen, H. Levring, WinXCom - a program for calculating X-ray attenuation coefficients, Radiat. Phys. Chem. (2004) 653–654, https://doi.org/10.1016/j.radphyschem.2004.04.040.
[26] J.E. Martin, Phys. Radiat. Protect. (2011), https://doi.org/10.1002/9783527667062.
[27] J.J. Duderstadt, L.J. Hamilton, Nuclear reactor analysis, Mech. Eng. 31 (1976) 138–142, https://doi.org/10.1109/TNS.1977.4329257.
[28] Jin I. Suk, Chang N. Park, Soon H. Hong, Young G. Kim, Development and properties of tungsten-bearing stainless maraging steels, Mater. Sci. Eng. A. 138 (1991) 267–273, https://doi.org/10.1016/0921-5093(91)90696-K.
[29] N.H. Heo, H.C. Lee, Effect of tungsten addition on the ductile-brittle-ductile transition in Fe-8Mn-7Ni-W maraging steels, Scripta Metall. Mater. (1995), https://doi.org/10.1016/0956-716X(95)00439-3.